# Acoustic normal mode fluctuation statistics in the 1995 SWARM internal wave scattering experiment

Robert H. Headrick, James F. Lynch, John N. Kemp, et al.

Citation: The Journal of the Acoustical Society of America **107**, 201 (2000); doi: 10.1121/1.428563
View online: https://doi.org/10.1121/1.428563
View Table of Contents: https://asa.scitation.org/toc/jas/107/1
Published by the Acoustical Society of America

# Acoustic normal mode fluctuation statistics in the 1995 SWARM internal wave scattering experiment

Robert H. Headrick,[a] James F. Lynch, John N. Kemp, Arthur E. Newhall, and Keith von der Heydt
*Woods Hole Oceanographic Institution, Woods Hole, Massachusetts 02543*

John Apel
*Global Ocean Associates, PO Box 12131, Silver Spring, Maryland 20908*

Mohsen Badiey
*Ocean Acoustic Laboratory, Graduate College of Marine Studies, U. Delaware, Newark, Delaware 19716*

Ching-sang Chiu
*Naval Post Graduate School, Monterey, California 93943*

Steve Finette, Marshall Orr, Bruce Pasewark, Alton Turgot, and Steve Wolf
*Naval Research Laboratory, Washington DC 20375-5350*

Dirk Tielbuerger
*Forschnungsanstalt der Bundeswehr für Wasserschall und Geophysik, Klausdorfer Weg 2-24, 24148 Kiel, Germany*

(Received 21 July 1997; revised 21 July 1998; accepted 13 September 1999)

In order to understand the fluctuations imposed upon low frequency (50 to 500 Hz) acoustic signals due to coastal internal waves, a large multilaboratory, multidisciplinary experiment was performed in the Mid-Atlantic Bight in the summer of 1995. This experiment featured the most complete set of environmental measurements (especially physical oceanography and geology) made to date in support of a coastal acoustics study. This support enabled the correlation of acoustic fluctuations to clearly observed ocean processes, especially those associated with the internal wave field. More specifically, a 16 element WHOI vertical line array (WVLA) was moored in 70 m of water off the New Jersey coast. Tomography sources of 224 Hz and 400 Hz were moored 32 km directly shoreward of this array, such that an acoustic path was constructed that was anti-parallel to the primary, onshore propagation direction for shelf generated internal wave solitons. These nonlinear internal waves, produced in packets as the tide shifts from ebb to flood, produce strong semidiurnal effects on the acoustic signals at our measurement location. Specifically, the internal waves in the acoustic waveguide cause significant coupling of energy between the propagating acoustic modes, resulting in broadband fluctuations in modal intensity, travel-time, and temporal coherence. The strong correlations between the environmental parameters and the internal wave field include an interesting sensitivity of the spread of an acoustic pulse to solitons near the receiver.  [S0001-4966(00)00601-9]

PACS numbers: 43.30.Re, 43.30.Bp [DLB]

## BACKGROUND

One of the hallmarks of the shallow water acoustic environment is its variability. Due to the importance of bottom interaction in shallow water, much attention has been paid to the variability of the bottom geology and the geoacoustic parameters of the bottom. However, in recent years, it has been recognized that the water column and its fluctuations also have a large impact on modulating acoustic signals in shallow water. Of particular interest has been the internal wave field, which can impress large fluctuations on shallow water signals, both in amplitude and phase/travel time. These fluctuations have important implications for array signal processing for both source localization and medium (inverse problem) studies.

One of the first indications of strong internal wave induced fluctuations came from the Yellow Sea work of Zhou and his co-workers, where anomalously large, frequency and azimuth dependent propagation losses were noted in tandem with high internal wave activity.[1,2] Zhou and other investigators postulated a ''Bragg resonant internal wave scattering plus bottom loss'' mechanism to explain this important observation.[1–4] However, the Yellow Sea data were not detailed enough, particularly the physical oceanography, to firmly prove or disprove this propagation loss hypothesis (or any other such reasonable hypothesis). The need for further higher resolution data was soon recognized. In order to understand both the acoustic scattering and losses produced by coastal internal waves, and their physical oceanography

[a]Robert H. Headrick was associated with the MIT/WHOI Joint Program in Oceanography and Oceanographic Engineering during the performance of this work. He is currently on active duty in the U.S. Navy.

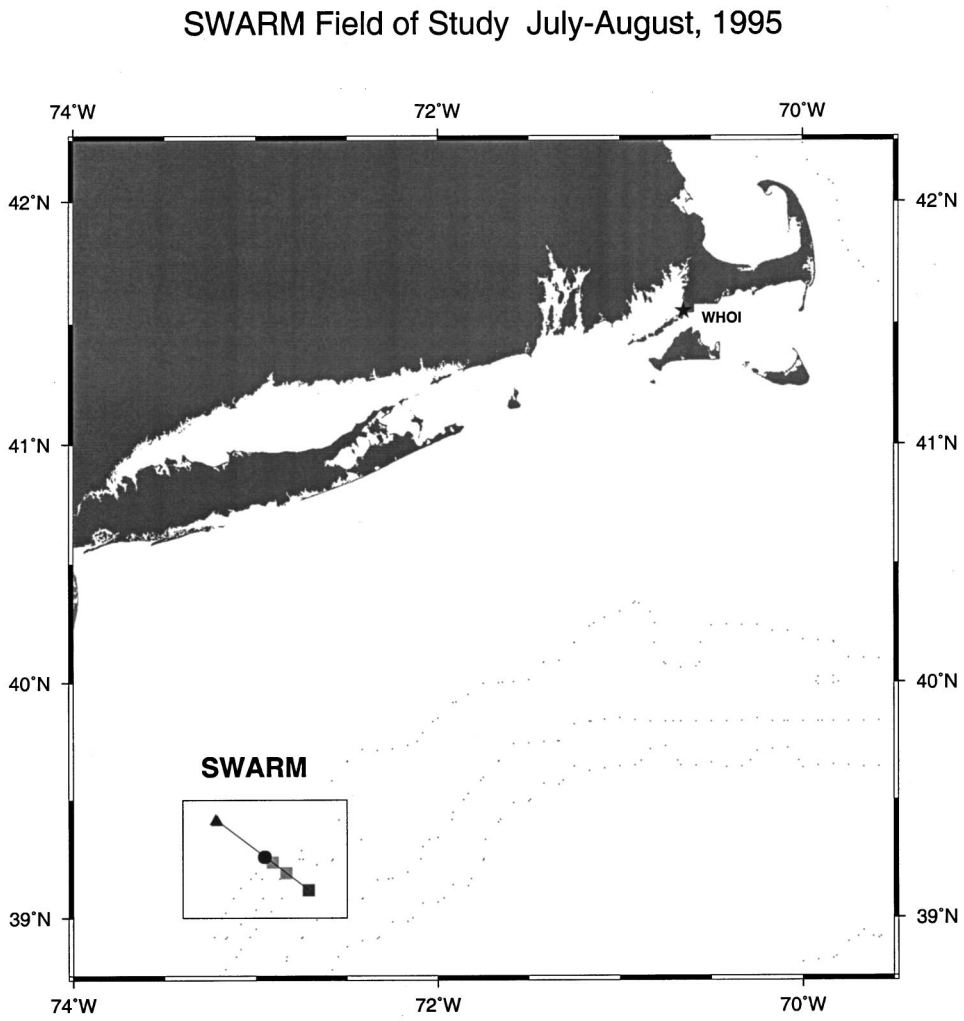


FIG. 1. Locations of acoustic moorings. The tomography sources, moored in close proximity, are a pair, 224 Hz and 400 Hz. The receiver is the 16 element WHOI vertical line array (WVLA). Coastal shelfbreak (at 200-m isobath) is main producer of the shoreward-propagating internal wave field affecting the acoustics transmissions.

(which is not perfectly known, especially for nonlinear coastal internal waves), a number of focused experiments were performed in the ensuing years. A semi-inclusive list of such experiments would include: (1) the 1995 SWARM experiment, which concentrated on acoustic pulse amplitude and travel-time variations as well as the physical oceanography of the nonlinear internal wave field;[5] (2) the 1995 STANDARD EIGER experiment, which looked at the issue of azimuthal variations in the acoustic field due to cnoidal, nonlinear waves;[6] (3) the Intimate '96 experiment, which examined the effects of the M2 internal tide (internal waves at M2 semidiurnal tidal frequency);[7] (4) the 1996–97 PRIMER experiments, which simultaneously examined both internal wave and coastal front effects on acoustic propagation;[8,9] (5) the 1995–96 SESAME I and II experiments, which had goals similar to those of the PRIMER experiments;[10] (6) the Strait of Gibraltar tomography experiment, which looked at scattering of acoustic energy for paths along the crests of nonlinear soliton trains;[11] and (7) the Yellow Sea follow-on experiment, in which Zhou and his colleagues (both from the U.S. and China) reconfirmed and extended their initial Yellow Sea measurements.[12] In addition, there have recently been a number of strictly physical oceanographic studies looking at the nature of the coastal internal wave field, which is quite different from the deep ocean field; however, discussion of these is beyond the scope of the present paper.

Our discussions in this paper will focus on the first experiment in our above list, the SWARM (Shallow Water Acoustic Random Medium) experiment. This experiment featured the highest resolution physical oceanography and acoustics combination achieved to date, which was necessary to understand acoustic fluctuations. In particular, we will focus on the travel-time fluctuations impressed upon acoustic pulses by the shallow water internal wave field. These include both the ''wander'' of the pulse (a change of pulse travel-time without change of pulse shape, an adiabatic mode effect) and the pulse ''spread'' (a change in pulse shape, due to mode coupling). The problem of the amplitude fluctuation of the fields, which was also measured in the SWARM experiment, is briefly treated here. In the main, however, this latter topic is outside the scope of this paper. We refer the reader mainly interested in internal wave induced amplitude fluctuations to the recent papers by Creamer, Tielbuerger *et al.*, Tang and Tappert, and Preisig and Duda.[13–16]

Our paper is organized as follows. In Sec. I, we present the description of the SWARM experiment, focusing on the mooring positions and their relation to the internal wave oceanographic field. In Sec. II, we discuss the characteristics of the acoustic data collected, including key elements of the

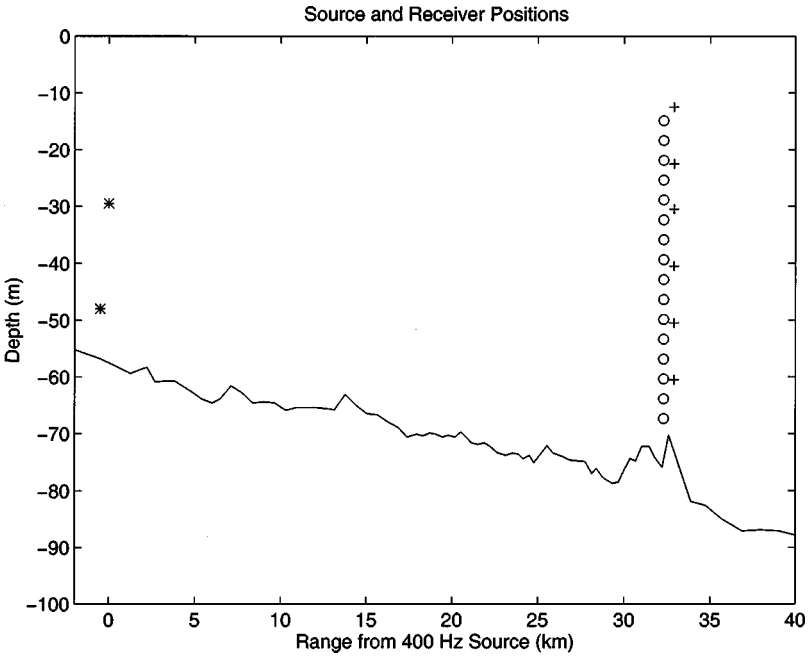


FIG. 2. Source positions are noted by ''*.'' The 400-Hz source is the shallower of the two. WVLA hydrophone positions are noted by ''○'' and the thermistors on the array are marked as ''+.''

subsequent data processing. Attention is paid to the mode filtration issue, as we later analyze data on a mode-by-mode basis. Section III of the paper treats the temporal variability observed in the mode filtered pulse arrivals, particularly their spread, wander, and bias. The strong correlation of these fluctuation statistics to the details of the internal wave field is one of the main results of the paper. This section also contains some analysis of the temporal coherence time of the acoustic modes, as well as a brief look at their amplitude fluctuations. Our final section, Sec. IV, contains a brief synopsis of the paper's results, our conclusions to date, and some thoughts on future directions for such work. The Appendix contains a short derivation showing how solitons near the acoustic receiver have the largest effect on time spreading, an effect noted in the data and dubbed ''near receiver dominance.''

## I. EXPERIMENT DESCRIPTION

The SWARM experiment[5] was conducted off the coast of New Jersey near the continental shelfbreak in July and August of 1995. The experiment was primarily dedicated to understanding acoustic normal mode scattering effect due to both linear internal waves and nonlinear solitary internal waves (solitons) in shallow water, and so was performed in late summer in order to see the strongest possible internal wave effects. In order to quantify the physical oceanography as well as the acoustics, the experiment included a myriad of acoustic and ocean environmental sensors; these sensors, their sampling schemes, and a complete overview of the data they produced in SWARM are given in Apel *et al.*[5] The present paper is chiefly concerned with the analysis of acoustic mode travel time data taken from the 16 element WHOI vertical line array (WVLA). Its mooring location, in about 70 m of water, is shown in Fig. 1. A pair of tomography sources, with center frequencies 224 Hz and 400 Hz, were moored for nearly three weeks 32 km shoreward of the WVLA receiver, such that the acoustic path was anti-parallel to the primary propagation direction for shelf generated internal wave solitons. Figure 2 shows a side view of the experiment, emphasizing the array extent in the water column. The temperature profile at the WVLA was monitored by six thermistors attached to the array at various depths. These temperature sensors, measuring twice per minute, gave good temporal resolution of the internal wave fluctuations and adequate spatial resolution in the vertical direction.

The SWARM region was well suited for an internal wave experiment. The internal solitary wave packets that we desired to study are so plentiful in summer that a nearly continuous stream of solitons would pass over a fixed instrument in the course of several hours. This is illustrated in Fig. 3, in which the array of thermistors attached to the WVLA records the passage of *many* waves over a 6-h period.

The mixture of time and space in this figure creates a distorted view of the soliton shapes. In terms of physical dimensions, typical soliton phase speeds of between 0.6 and 0.8 m/s would require on the order of a tenfold increase in the horizontal dimension of the lowest panel in Fig. 3 to achieve a properly scaled representation of a soliton. The resulting horizontal gradients in sound speed are still quite strong, however, and the level of soliton activity was more than sufficient to ensure some highly coupled mode arrivals at the WVLA. The magnitude of the horizontal gradient at mid-depth can be seen in Fig. 4, which shows the sound speed in the middle of a typical soliton and just outside it.

## II. SWARM ACOUSTIC DATA CHARACTERISTICS

The 400-Hz (100-Hz bandwidth) tomography source produced a 511 digit, phase-modulated signal sequence with a digit length of 4 cycles, giving a total of 5.11 s per sequence. The sequence was repeated 23 times during each transmission, for a total transmission time of 117.53 s. (We only used 22 of the transmissions in practice.) The 400-Hz transmissions started on the hour and were repeated every 6 min. They were received at the WVLA about 22 s later.

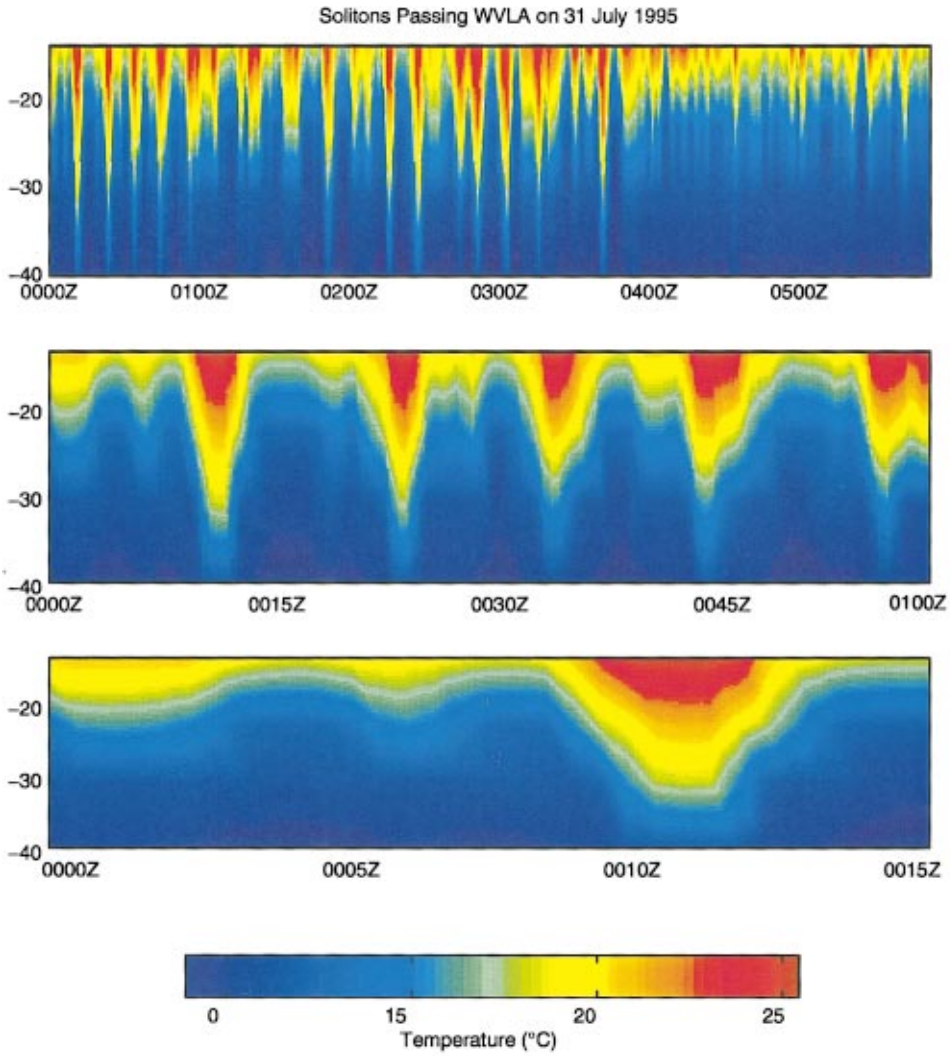


FIG. 3. Time and space interpolation of four thermistor records. The thermistors were attached to the WVLA at water depths of 12.5, 20.5, 30.5, and 40.5 m and sampled at 30-s intervals.

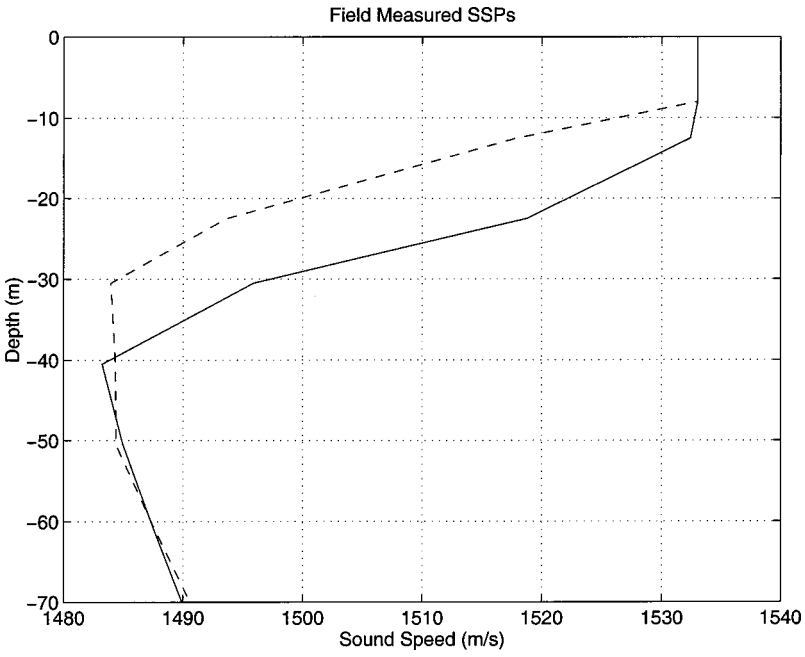


FIG. 4. Sound speed profiles in the center of a typical soliton (solid) and just outside it (dashed). Horizontal sound speed gradients of up to 25 m/s over 100 m can be inferred from such profiles.

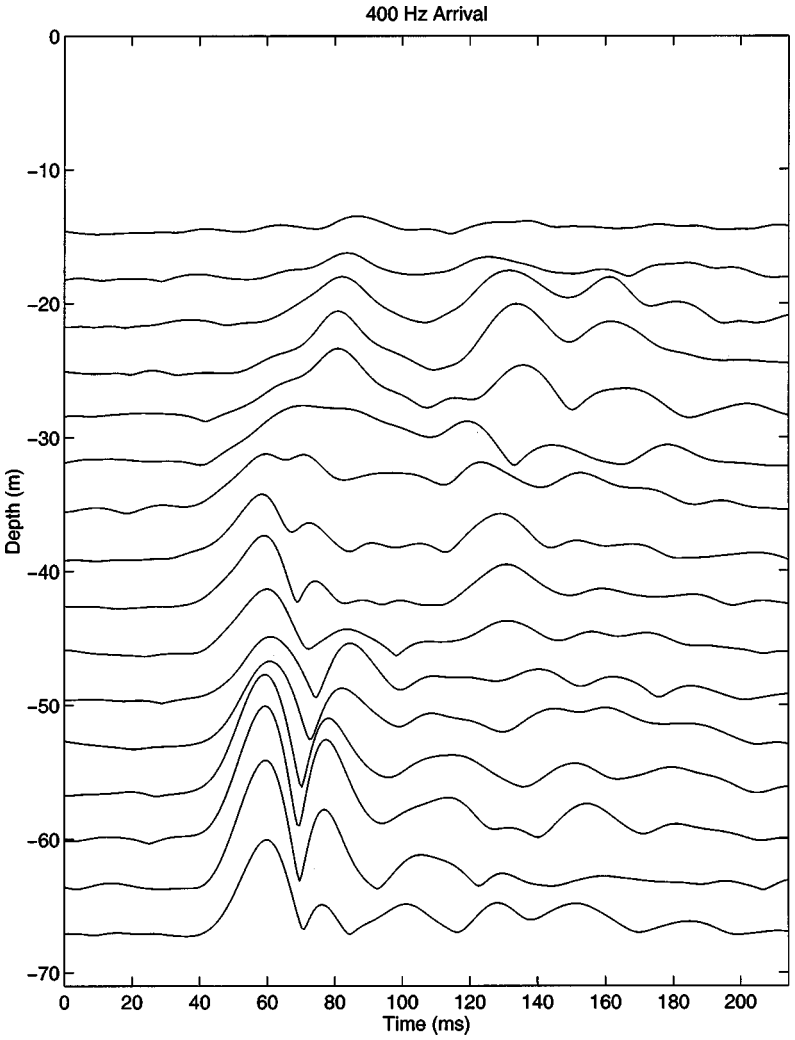


FIG. 5. Typical 400-Hz arrivals observed at the WVLA hydrophones during SWARM. Plot shows pressure field amplitude in linear units.

Figure 5 shows a typical set of 400-Hz pulse-compressed arrivals for the 16 hydrophones at the WVLA. The term ''typical'' is used rather loosely here, as the scattering from internal waves in the waveguide causes significant temporal variability in the individual hydrophone arrivals. What *is* typical here is that a set of arrivals generally consists of an early packet of energy with a mode one amplitude and phase depth dependence followed by a signal of about about 100-ms duration having ''mixed mode'' characteristics.

The 224-Hz arrivals are similar, but the narrower bandwidth (16 Hz) yields a broader pulse width ($\cong$60 ms). The 224-Hz source produced a 63 digit, phase-modulated signal with a digit length of 14 cycles, with period 3.9375 s per sequence. The sequence was repeated 30 times during each transmission, for a total transmission time of 118.125 s. The transmissions were repeated every 5 min, starting on the hour. They were received at the WVLA about 22.5 s later.

We should note in closing this section that this sampling schedule, while reasonable for looking at internal waves, was still somewhat sub-optimal. Although the 5- and 6-min repetition rates were perfectly adequate for M2 tidal period (12.42 h) studies, they somewhat aliased the interval between individual solitons, which are typically on the order of 4 to 10 min. A 100% duty cycle transmission would have been preferred, but battery limitations in the source and (circa 1995) disk storage limitations in the receiver precluded that option.

### A. Mode filtering of received signals

The modal analysis of 400-Hz acoustic arrivals at the WVLA begins by treating the acoustic signal at each hydrophone as a sum of vertical modes

$$p_h(t)=\sum_{n=1}^{N} A_n(t)\phi_n(z_h), \tag{1}$$

where $\phi_n(z)$ is the modal pressure depth function, $A_n(t)$ is the mode coefficient, and $z_h$ is the depth of the $h$th hydrophone. The number of propagating normal modes, $N$, as well as the mode shapes themselves are frequency dependent.

The six thermistors on the WVLA, which are sampled every 30 s, adequately provided the water column sound speed profiles needed for computing a time-dependent set of 400-Hz mode shapes using the KRAKEN[17] normal-mode code. (Bottom parameters are taken from Apel *et al.*[5]) The basis for this code, a numerical normal-mode solution of the Helmholtz equation at angular frequency $\omega$,

$$[\nabla^2+k^2(r,\omega)]p(r,\omega)=0, \tag{2}$$

TABLE I. Auto and cross-mode rejection levels for best case, worst case, and average mode arrival/filter scenarios.

| Input mode | Auto and cross-mode rejection levels (dB) | | | | | | | | | | | |
|---|---|---|---|---|---|---|---|---|---|---|---|---|
| | Best filter | | | | Worst filter | | | | Average filter | | | |
| | 1 | 2 | 3 | 4 | 1 | 2 | 3 | 4 | 1 | 2 | 3 | 4 |
| 1 | 0 | 47 | 46 | 40 | 0 | 13 | 24 | 32 | 0 | 31 | 35 | 36 |
| 2 | 49 | 0 | 34 | 31 | 13 | 1 | 11 | 20 | 31 | 1 | 22 | 26 |
| 3 | 46 | 34 | 0 | 26 | 24 | 11 | 1 | 11 | 34 | 22 | 1 | 18 |
| 4 | 40 | 31 | 26 | 1 | 32 | 21 | 11 | 2 | 36 | 26 | 18 | 1 |

where $p(r,\omega)$ is the Fourier component of the pressure field, can be found in Jensen *et al.*[18]

The KRAKEN mode shapes are orthonormal in the sense that,

$$\int \frac{\phi_m(z)\phi_n(z)}{\rho(z)}dz = \delta_{mn}, \tag{3}$$

so given $p(z,t)$,$A_n(t)$ can be readily computed by applying the operator

$$\int (\cdot)\frac{\phi_n(z)}{\rho(z)}dz. \tag{4}$$

Since the pressure field, $p(z,t)$, is only sampled at the 16 hydrophone locations, the integral computation of the mode coefficients, $A_n(t)$, must be approximated by

$$A_n(t) \simeq \sum_{h=1}^{16} \frac{p(z_h,t)\phi_n(z_h)\Delta z}{\rho(z_h)}, \tag{5}$$

where $\Delta z$ is the spacing between hydrophones. This discrete sum is easily implemented through matrix multiplication of mode shape vectors with 16 channel hydrophone data vectors (i.e., narrow-band direct-projection mode-filtering). A more accurate filter would take into account the frequency dependence of the modal depth functions over the bandwidth of the acoustic arrivals, but the effects were shown by our calculations to be minimal and thus the increased computation time was not warranted.[19]

The direct projection method works well for the low modes that are adequately sampled by the WVLA. A typical SWARM mode 1 shape will yield,

$$\sum_{h=1}^{16} \frac{\phi_1(z_h)\phi_1(z_h)\Delta z}{\rho(z_h)} = 0.9989, \tag{6}$$

very close to the ideal output of 1.0. Higher order modes have more energy outside the depths sampled by the WVLA, so the above projection-filtration scheme degrades, yielding outputs of 0.9949, 0.9881, 0.9803, 0.9681, 0.9269, and 0.8243 for modes 2 through 7, respectively. The higher order modes suffer more from partial vertical coverage than they do from undersampling, so that a simple output gain factor (such as one obtained by dividing the filter output by its projection-filtration level) may be useful if level comparisons between mode arrivals are to be made. However, an output gain factor will not provide relief from modal crosstalk, which is inherent with undersampling and partial coverage.

Two other factors to consider in mode-filter performance are array tilt and deviations between the calculated and actual modal depth functions at the receiver. Tilt for the WVLA seldom exceeds 1°, except during the passage of a particularly large soliton where it may approach 2°.[19] Time offsets between the actual modal depth functions at the WVLA and the mode-filter being used can range from 0 to 42 s.[19] These factors, and thus the levels of cross-mode rejection, are time dependent, i.e., we see fluctuations in the cross-mode rejection performance of the mode-filters. Worst case assumptions can drop the nearest neighbor (adjacent mode order) rejection levels down to the 10-dB level, but on average the performance is in the 20-dB range.

Table I gives best case, worst case, and average cross-mode rejection estimates for the mode-filters. The best case scenario assumes zero tilt and no time offset, and the worst case assumes a constant tilt of one degree and a 30-s offset between the arrivals and the mode-filters. As stated before, tilts may exceed 1 m from time to time and time offsets of up to 42 s are possible, so the ''true worst case'' is a fairly elusive concept; mode shapes can only be tabulated at 30-s intervals, and the tail of the tilt distribution function is difficult to quantify. Given all this, the term ''nearly worst case'' might be better for the tabulation presented above.

### B. Acoustic impact of solitons

Internal wave induced coupling between acoustic normal modes, combined with differences in the acoustic modal group velocities, causes the time spreading of pulses as energy is transferred between different acoustic modes. In the SWARM waveguide, mode one usually has the highest group speed (see Table II), so that energy which transits in other modes for a portion of the source-to-receiver trip and then couples to mode one is of necessity delayed with respect to energy that traveled exclusively in mode one. This

TABLE II. Calculated modal group speeds at 400 Hz for sound speed profiles inside and outside the soliton shown in Figs. 3 and 4. The calculation of group speeds was performed using a range independent model.

| Mode | Group speeds | |
|---|---|---|
| | Outside soliton | Inside soliton |
| 1 | 1484.1 | 1484.2 |
| 2 | 1483.2 | 1482.8 |
| 3 | 1481.1 | 1480.0 |
| 4 | 1478.2 | 1477.7 |
| 5 | 1475.6 | 1475.2 |
| 6 | 1472.9 | 1479.7 |
| 7 | 1472.2 | 1488.6 |
| 8 | 1471.4 | 1488.4 |

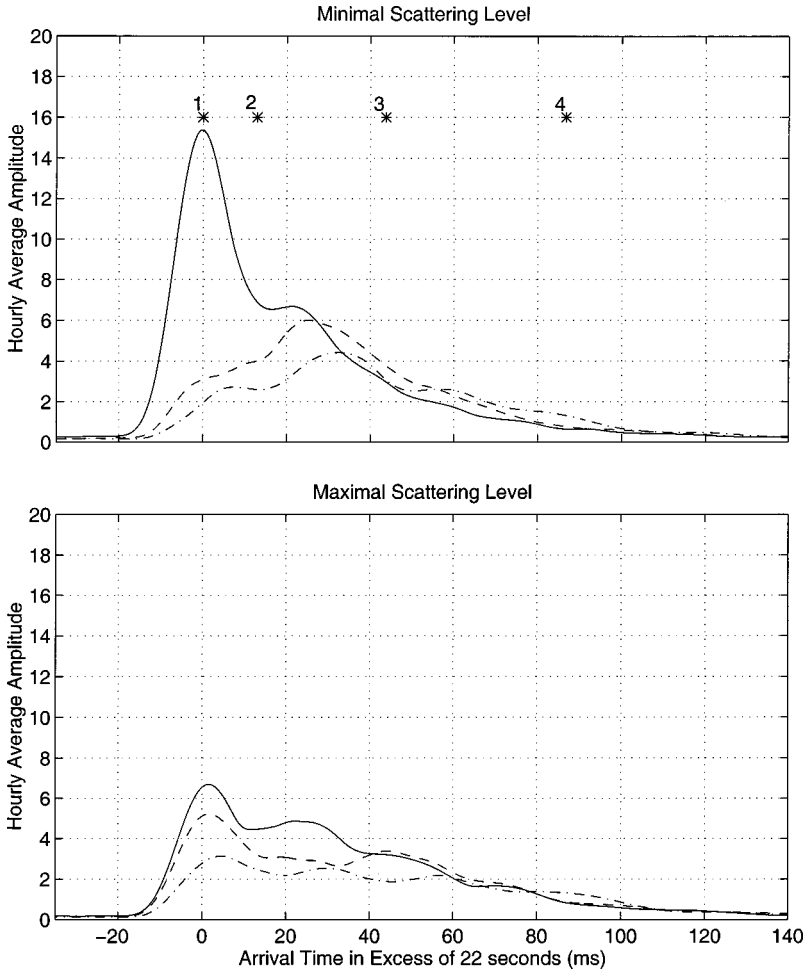


FIG. 6. Two different 1-h incoherent averages of mode one (solid), mode two (dashed), and mode three (dot-dash) filtered outputs. The top figure represents a period of minimal scattering of energy between modes and the lower figure a period of maximal scattering. The periods are separated by about 12.5 h. The numbered asterisks in the top figure represent predicted adiabatic mode arrival times for modes 1–4.

causes the spread of mode one energy to be all in one direction (i.e., there is a positive bias in the mean and median travel time of mode one energy relative to an unscattered mode one arrival). Higher order modes may have some energy arriving earlier (from traveling part of the path in lower order modes) and some arriving later (from traveling part of the path in higher order modes); thus there may be negative, positive, or even zero bias in the travel-time of the spread high order mode arrivals.

The effect of the spreading/smearing of energy on the intensity of mode one arrivals is two-fold. First, the spreading itself reduces the intensity of the mode one peak and, second, the attenuation level for higher order acoustic modes is greater, so energy that transits even a portion of the waveguide in some mode higher than mode one will suffer increased attenuation. This second effect was first proposed to explain intensity fluctuations observed in previous shallow water CW experiments.[1,20]

The amount of mode spreading and attenuation is quite variable. To illustrate this variability, Fig. 6 shows two different 1-h incoherent averages of mode 1–3 filtered outputs. The pulse distortion increases very dramatically over the 12.5 h separating these two averages.

## III. TEMPORAL FLUCTUATIONS IN MODE ARRIVAL STATISTICS

Figure 6 provides a good illustration of the variability inherent in the mode filtered outputs of the acoustic data. Some of the important observables in the acoustic data are spread, bias, wander, intensity, and temporal coherence. All of these statistics are interrelated to varying degrees, and with the exception of wander, they are all sensitive to the numbers and location of solitons in the waveguide. We now examine them in some detail.

### A. Spread, bias, and wander

#### *1. 400-Hz mode 1 arrivals*

We first look at the wander in travel-time of acoustic mode one. The nature of the SWARM waveguide is such that this mode generally has the highest group speed, making the energy that travels nearly exclusively in mode one the earliest possible arrival for most transmissions. This energy is referred to as the pseudo-adiabatic mode one arrival (PAM1).[19] It is not always the strongest peak in the envelope of a mode one arrival, but energy arrives at or near the PAM1 arrival time strongly enough so that distributions of mode one peak arrival times have observable leading edges. There are exceptions. During the early hours of day 212, at the WVLA, mode two has a higher group velocity than mode one; if and when this is the case for the majority of the waveguide, the PAM2 arrival will precede the PAM1 arrival, allowing for some positively biased mode one energy. The leading edge of mode one, when observable, is quite useful

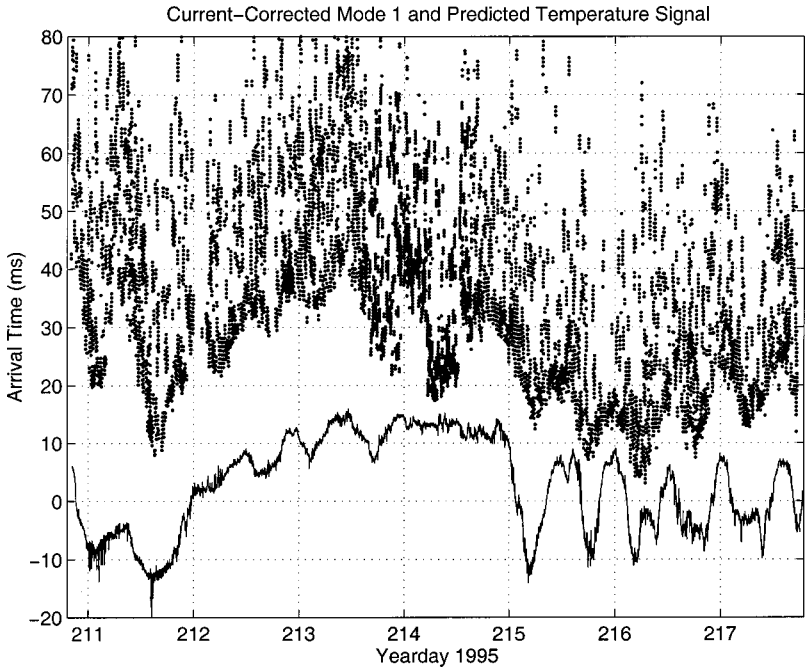


FIG. 7. Predicted temperature fluctuation effects on PAM1 arrival time (solid curve) plotted along with the distribution of ''current-corrected'' acoustic peak arrival times (dots). The peaks are picked from over 32 000 mode one arrival envelopes that are similar to those shown in Fig. 6. Only the highest peak from each envelope is plotted. The solid curve prediction is zero mean (by definition) and is offset from the acoustic data for convenience. Generally good agreement between the prediction and the leading edge of the acoustic pulses in noted.

in that its travel-time wander is a sensitive measure of the oceanic heat content variation along the path connecting the source and receiver.

The ''current-corrected'' distribution of SWARM mode one peak arrival times, which is our cleanest data set for the modes, is shown in Fig. 7. The arrivals have a fairly sharp leading edge; there is little or no indication of negatively biased peaks. [The current-correction to travel-time is derived from a bottom moored current meter near the WVLA. Specifically, the predicted travel-time fluctuations (order $\pm 3$ ms) obtained from applying the measured barotropic (depth independent) currents (predominantly M2 tidal, i.e., the strong 12.42-h period semidiurnal tidal component) to the entire acoustic path were subtracted from raw peak arrival times.] The mode one wander, as seen in Fig. 7, is substantial, and a good portion of it can be correlated with temperature fluctuations in the vicinity of the WVLA. These fluctuations were logged in thermistor records from the WVLA and three dedicated thermistor strings moored in a cluster 4.5 km shoreward of the WVLA. The solid curve in Fig. 7 is obtained by using the average change in sound speed seen at seven of these thermistors to calculate travel-time variations. The seven thermistor records used (three from the WVLA, four from the dedicated strings) were in the depth band of interest for acoustic mode one (40–60 m) and judged to be reliable records. The foot of the shelfbreak front, which has been observed in CTD profiles to extend across the position of the WVLA, seems a very likely source of the temperature fluctuations.[5] The actual range between the thermistors used is only 4.5 km, but the effects may be reasonably extrapolated farther along the acoustic path, since the foot of the front extends somewhat farther inshore. The choice we made of 8 km provides a level of predicted variance close to that observed in the acoustic data. However, the PAM1 wander occurring on yearday 214 is a clear indicator that large temperature fluctuations are not entirely restricted to the frontal area around the WVLA, and it is likely that changes in temperature along the entire 32-km path contribute at various times and in varying degrees to the acoustic mode one wander.

We next look at the spread of the mode one arrival at 400 Hz. The range and variability of positive bias seen in the Fig. 7 peak arrival distribution is indicative of significant time spreading in the mode one arrival patterns. Spread is perhaps the simplest quantitative measure of signal distortion and also is a clear indicator of coupled mode scattering being produced by the waveguide.

Spread is conceptually simple, yet the choice of which mathematical definition of spread is ''best'' to use is somewhat subjective. Four typical measures that could be considered are: (1) the interquartile range (IQR) of the arrival envelope; (2) the standard deviation of the arrival envelope; (3) the absolute value of the peak minus the mean arrival time; and (4) the standard deviation of the peak times in a 22 sequence transmission. This list is obviously not exhaustive but is a good selection of the possibilities. We will eventually concentrate on IQR in our work, where the IQR time spread is defined here as the difference in time between where 25% of the total pulse integrated amplitude (always positive, i.e., absolute value of amplitude) has arrived and where 75% of the total pulse integrated amplitude has arrived. One can use energy definitions of IQR as well; we chose amplitude simply for ease of processing.

Using method one, the IQR, analysis results for the WVLA mode one arrival spread are shown in Fig. 8. The upper frame of Fig. 8 is a plot of the spread averaged over each 22-sequence transmission, while the lower frame includes five different bin averages ranging from 1.4 to 4.1 h for comparison. The upper frame of Fig. 8 reveals significant spread variability over time scales ranging from several minutes up to semidiurnal tidal oscillations. The M2 tidal oscillations, along with other low frequency signals, are readily evident in the longer bin averages shown in the lower frame.

The second method of estimating spread, standard de-

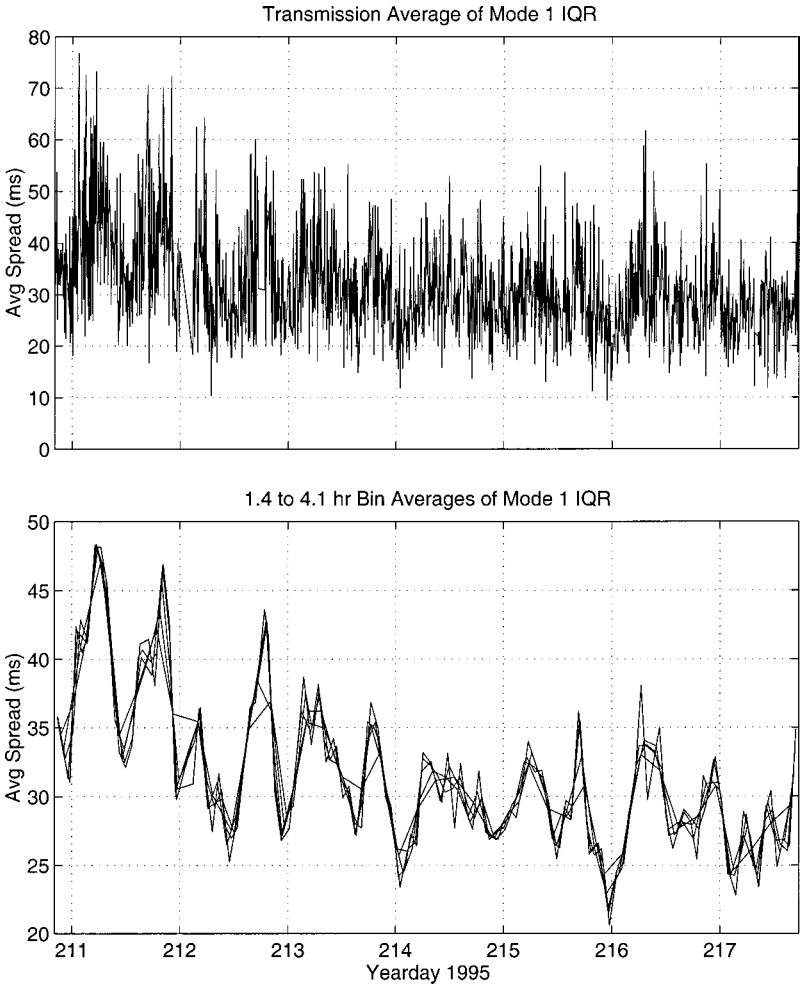


FIG. 8. Mode one arrival spread, as measured by the IQR of the arrival envelope (unscattered IQR is about 7.2 ms). The upper frame of Fig. 8 is a plot of the spread when averaged over each transmission (22 sequences per transmission). The lower frame shows bin averaged spreads for five bin widths ranging from 1.4 to 4.1 h.

viation, is very similar to the first; the main difference is in its sensitivity to outlying energy. The third method, absolute value of peak minus mean, strictly speaking, is more a measure of ''non-Gaussianess'' than a measure of spread, but these usually go hand-in-hand. Whereas the first three methods require evaluation of the arrival envelope, the fourth method, standard deviation of peak times, only requires the peak arrival times to be recorded. The tradeoff for this is that only one measurement can be obtained per transmission, as opposed to 22 per transmission for the other three.

Applying each of these methods to the mode one arrival records from SWARM produces varying degrees of similarity between methods. Using 1.4-h bin averages (see Fig. 8) as benchmarks, the following matrix of zero-lag cross-correlation values between the time series generated by the different methods can be constructed:

$$\begin{bmatrix} 1.00 & 0.97 & 0.85 & 0.57 \\ & 1.00 & 0.82 & 0.60 \\ & & 1.00 & 0.29 \\ & & & 1.00 \end{bmatrix}.$$

As expected, the correlation is the strongest between methods one and two, and the other combinations show limited similarity. The IQR will from here on be the primary method by which spread is measured.

We also looked at our Fig. 8 time series in the frequency domain. The spectra (not shown) reconfirm the existence of significant variability near the M2 semidiurnal tidal frequency. This tidal variability is consistent with our understanding of the most probable source of the spread in the arrivals: internal wave solitons associated with nonlinear M2 internal tides called ''solibores.'' [21]

The relationship between tides and soliton formation appears to be strong, but it is not simple, and it is certainly not linear; the numbers and sizes of solitons, as well as the extent of the internal tidal bores (long wavelength, nonlinear internal tide isotherm depressions) they are often associated with, can change dramatically from one tidal cycle to the next. This, coupled with multiple soliton-generation sites and the complicated relationship between acoustic spread and soliton density, produces a rather broad M2 line in the pulse spread spectrum. Figure 9 graphically illustrates this variability in the soliton packets from cycle to cycle. Figure 9 also displays another very important effect—the mean spread levels are seemingly controlled by the density of solitons in the near-receiver portion of the waveguide. The sensitive dependence of the pulse spreading to solitons near the receiver is an important point in this paper, as well as in the sequel paper to this one.[22] A brief explanation of the physics of why the spreading depends most crucially on near-receiver solitons is to be found in the Appendix of this paper; a more

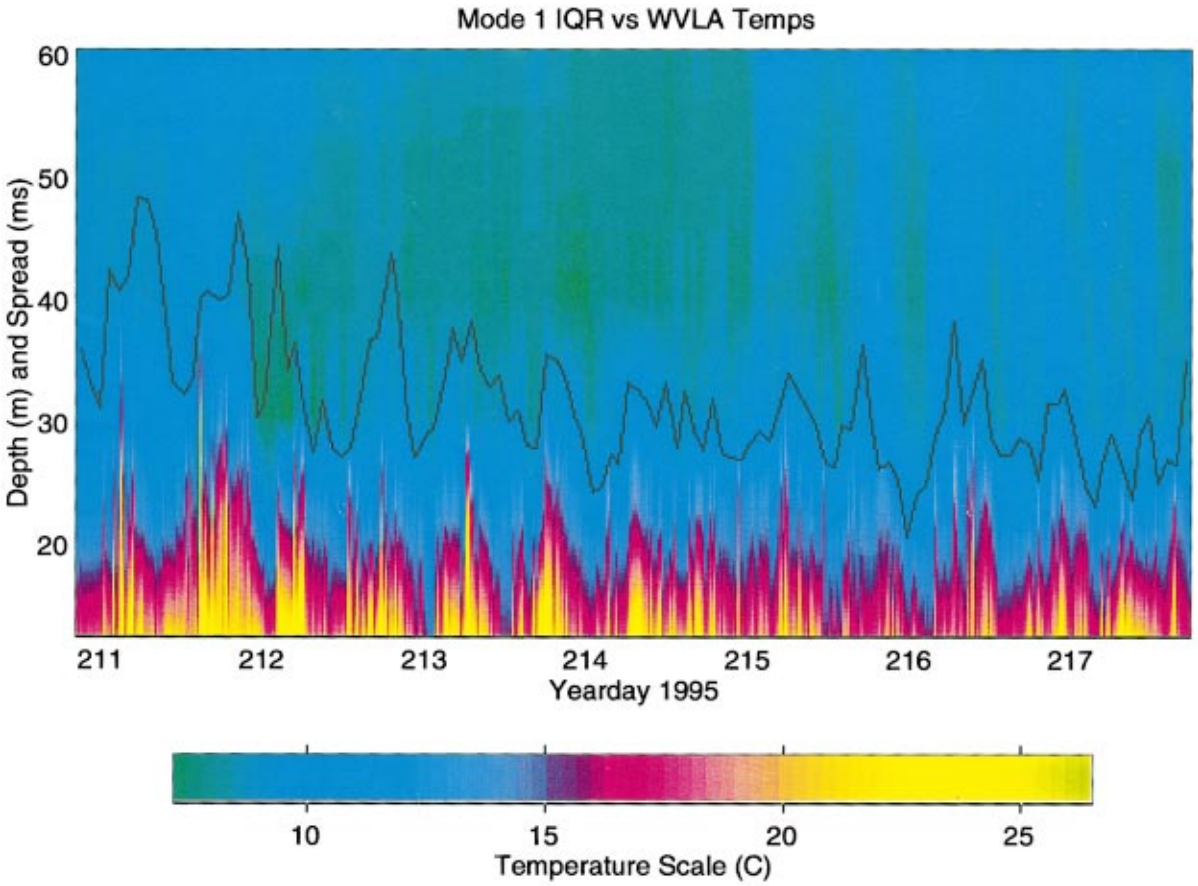


FIG. 9. WVLA temperature as function of time and depth overlaid by the 1.4-h bin averaged IQR estimate of mode one arrival spread at the WVLA. Both the variability in the fields and the correlation of the spread to the near-receiver temperature fluctuations are of note here.

detailed explanation can be found in the sequel paper.

To further understand the relationship between the oceanography and the acoustic spread and bias seen, we will look at the propagation of the solibores along our acoustic track. This oceanography and its relation to the sound speed field is most easily seen in the isotherm displacement records made by the thermistor strings placed along the acoustic path. (We have already looked at these records somewhat in examining the acoustic wander.) Since the majority of solitons in the SWARM region propagate anti-parallel to the acoustic path, one can assume, to first order, that most of the temperature disturbances seen at the WVLA will propagate in some fashion across the shelf toward the acoustic source region at speeds from 0.6 to 0.8 m/s.[19] To show this, Fig. 10 illustrates an analysis of three thermistor records from various locations along the acoustic path. The first is record is from a thermistor on the WVLA at a depth of 12.5 m. The second record, at a range of 5 km, is from a thermistor from Temperature String 598 at a depth of 17.5 m. The final record, at a range of 32 km, is from a thermistor on the Naval Research Laboratory (NRL) source mooring at a depth of 18 m. (The NRL source was moored about 0.6 km downslope from the 400-Hz tomography source. It did not function, but the thermistor pod on it did.) The diagonal lines on Fig. 10 correspond to a nominal solibore propagation speed of 0.8 m/s; this speed reasonably connects many of the tidal period disturbances evident in the three records, especially the low frequency M2 ''solibore envelope.'' Later portions of all three records (past yearday 214, e.g., see Fig. 9 for the WVLA record) have weaker M2 internal tidal signals that are hard to correlate between moorings. Assuming this fixed propagation velocity of 0.8 m/s anti-parallel to the acoustic path, the disturbances at the WVLA would reach the acoustic sources some 670 min later. Thus using Fig. 9, an inference can be made that the temperature profiles in the graph up to 670 min earlier than a given spread reading at time $t_0$, when converted to distance using 0.8 m/s, are a rough approximation to what the waveguide looked like at the time of the transmission. This inference is basically a ''frozen field,'' constant velocity advection approximation that follows Rubenstein and Brill.[20] Such an approximation ignores the the spatial and temporal evolution of the solibores,[23] but given that we did not have the extensive data needed to quantify the evolution of individual solibores, it is a reasonable, ''data based'' first approximation.

As mentioned, a visual analysis of Fig. 9 reveals a reasonable degree of correlation between mode one spread levels and soliton induced thermal activity near the receiver. The estimated WVLA-receiver-to-source transit time of 11.2 h is sufficiently short to place the bulk of the previous tidal cycle's solitons outside the acoustic path when a solibore packet of interest is in the region of the waveguide near the receiver. However, the situation reverses if slightly lower, but still reasonable, soliton propagation speeds are assumed; a speed of 0.6 m/s yields a receiver–source transit time of 14.9 h, placing two sets of solitons in the acoustic path at the

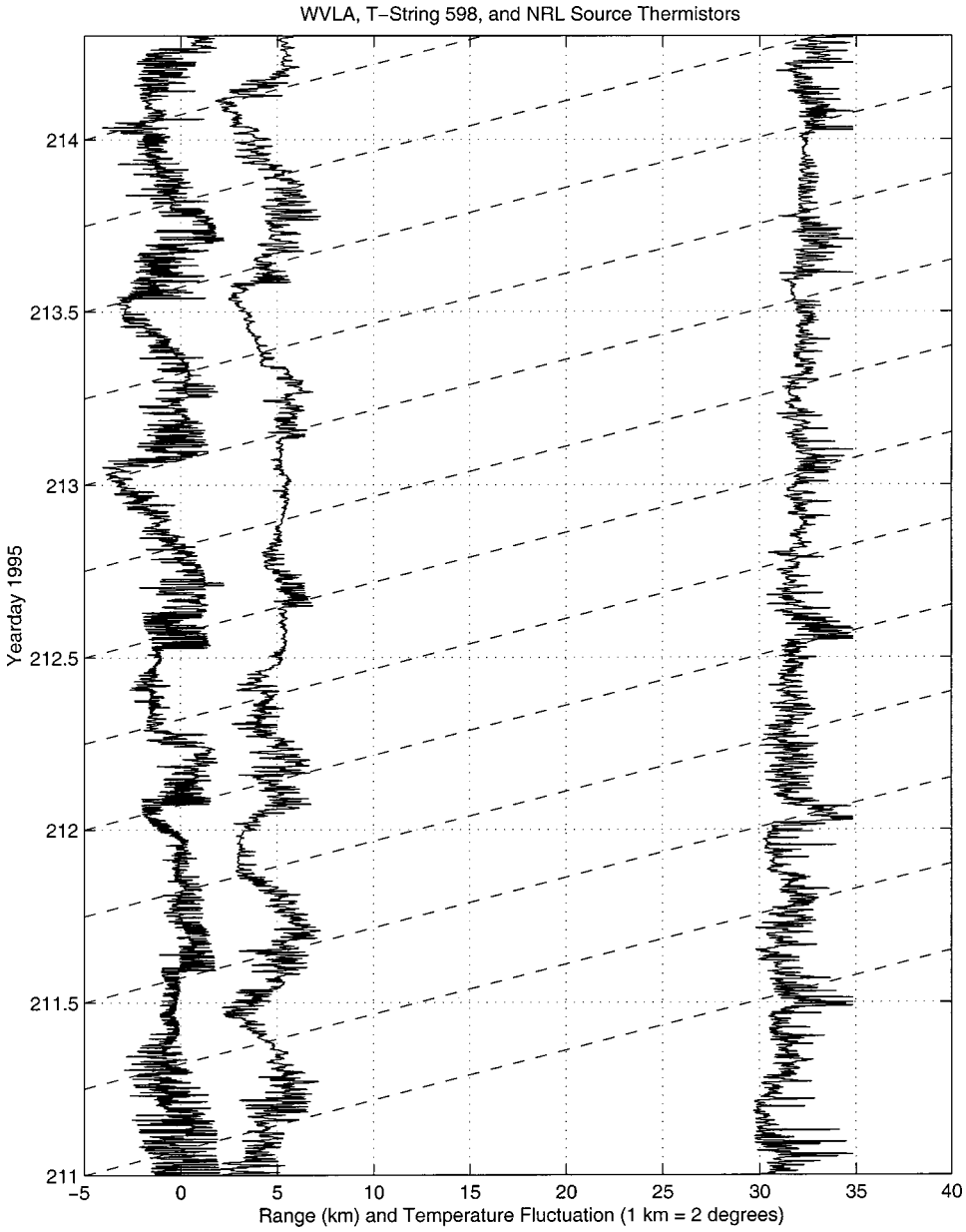


FIG. 10. The temperature fluctuations at three shallow thermistors plotted as a function of time, offset by their respective shoreward distances from the WVLA. The first is a thermistor on the WVLA at a depth of 12.5 m, the second at range of 5 km is a thermistor from Temperature String 598 at a depth of 17.5 m, and finally at a range of 32 km is a thermistor from the NRL source mooring at a depth of 18 m. The diagonal lines correspond to a propagation speed of 0.8 m/s.

times when large numbers of solitons are near the receiver. Also, it is observed that ''M2 arrival times'' of trains of solitons at a fixed point a few tens of kilometers shoreward from the shelfbreak fluctuate by $\pm 10-20$ percent, due to changes in oceanographic conditions. Thus 11.2 h is really just a mean of a distribution of solibore transit times between the WVLA and the source location. This is reflected in the Fig. 10 data, and implies that our present data thus cannot unambiguously differentiate between effects due to solitons near the acoustic sources and near the acoustic receivers. (The third array deployed, which failed due to flooding, would have been able to make such an unambiguous separation due to its shorter source-to-receiver path.) We thus must still appeal somewhat to physics arguments that the time spreading observed is due to near-receiver solitons, as opposed to solitons near the source. Again, we refer the reader to the Appendix and to our sequel paper.[22]

Even with an assumed 11.2-h transit time, it is difficult from Fig. 9 to exactly quantify correlations between soliton activity and spread levels visually. However, if the standard deviation of the temperature at 22.5-m depth over the previous 4.3 h (a reasonable binning time and ''much less'' than either the 11.2-h transit time or the 12.42-h M2 period) is used as a measure of soliton activity near the receiver, then we can see a clearer picture of the time series correlation, as shown in the upper panel of Fig. 11. A correlation level of 0.65 is obtained (see Fig. 11, lower panel). This level is rather good, given the inherent variability in the oceanographic field and the acoustic pulse shapes.

### 2. Higher modes

Peak arrival scattergrams for the higher order modes look similar to the mode one scattergram shown in Fig. 7. The scattergram data for the first four modes are summarized, using their leading edges and bin averaged mean arrival times, in the plots shown in Fig. 12. These figures show two more statistics with a strong M2 tidal influence. The

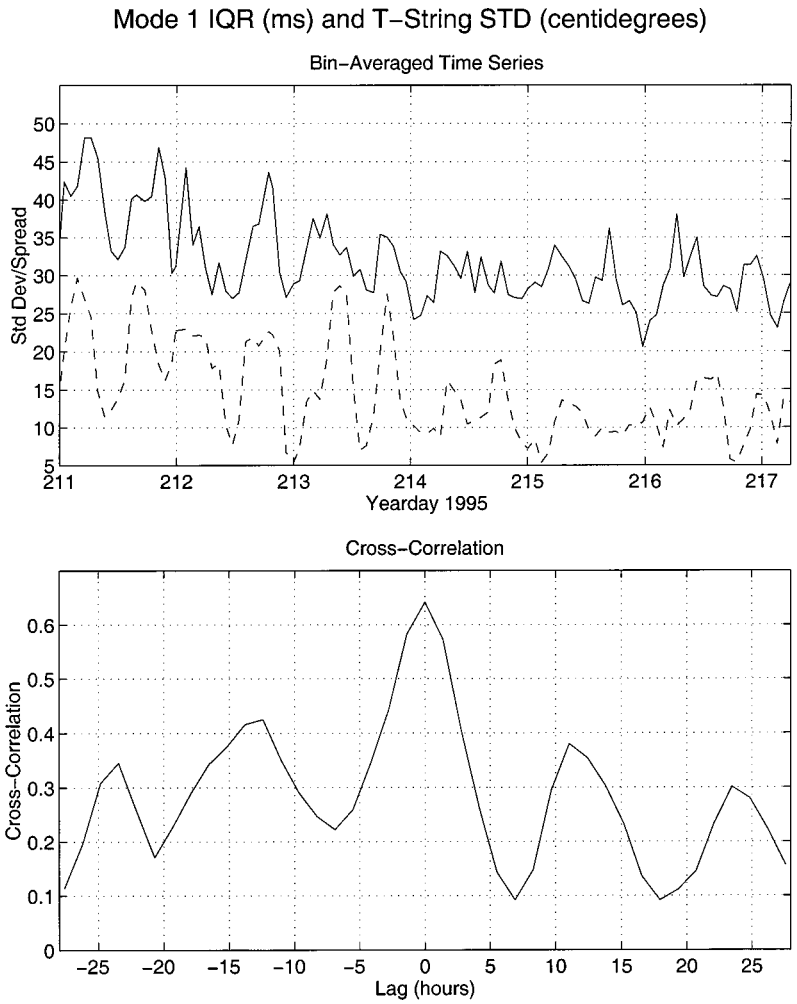


FIG. 11. The upper frame shows a comparison of 1.4-h bin averaged IQR levels for the SWARM data (solid line) and the standard deviation of the temperature at 22.5-m depth over the previous 4.3 h (dashed line). The standard deviation of the temperature is in tenths of a degree C to facilitate comparison with the IQR levels in milliseconds. The lower frame shows the cross-correlation of the two time series.

mean mode four arrival time has an M2 tidal variability that is greater than the tidal modulation of the PAM1 arrival (i.e., the peaks in the upper panel dotted line have larger amplitudes than the peaks in the lower panel solid line). These mean mode four arrivals are also negatively biased relative to the predicted PAM4 arrival, and are generally within 80 ms or less of the mode one leading edge (80 ms is the average difference between computer simulated PAM1 and PAM4 arrivals). In physical terms, this implies that the mode four arrival structure is more sensitive to mode coupling than is the mode one arrival structure, which is sensible, since mode four would be extremely weak (due to bottom attenuation) were it not for mode coupling.

Following Fig. 11 for mode one, Fig. 13 compares 1.4-h bin-averaged spread statistics for modes 2–4 to the standard deviation of the temperature at 22.5-m depth over the previous 4.3 h. The behavior of the mode two spread is very similar to the mode one behavior, and the correlation with the temperature statistic is equally strong. As the mode number increases past mode two, the tidal signal appears to decorrelate from our measure of ''near-receiver'' soliton activity. Physically, we believe that this is due to a larger fraction of the high mode energy being due to mode coupling whenever it is seen, so that it will have a more constant amount of spread versus clock time.

### *3. 224-Hz arrivals*

The 224-Hz tomography source, moored about 1000 m farther up the shelf, provides a second source of acoustic arrivals at the WVLA. The narrower bandwidth of the 224-Hz source yields a pulse width of about 60 ms versus the 10-ms pulse width of the 400-Hz signal.

The wider pulse width of the 224-Hz source no doubt contributes to the somewhat fuzzy distribution of 224-Hz mode one peak arrival times shown in Fig. 14. It is difficult to estimate just what portion of the variability in the 224-Hz peak arrival time wander should be attributed to measurement uncertainty associated with the broader pulse, but using the shape of the 400-Hz pulse leading edge as a guide, an uncertainty of around $\pm 5$ ms appears to be appropriate. A similar qualitative analysis of Fig. 7 leads us to believe the uncertaintity for the 400-Hz peak arrival times is less than about $\pm 2$ ms. An interesting feature of the Fig. 14 plot is the apparent divergence between the leading edges of the 224-Hz and 400-Hz distributions of peak arrival time. Frequency dependence in the mode one group velocity is not large enough to explain all of this divergence. One possibility is that the leading edge in the mode one 224-Hz arrivals may not be as strongly tethered to the PAM1 arrival time as is the case for the 400-Hz mode one arrivals.[19]

The time histories of the 224-Hz and 400-Hz bin aver-

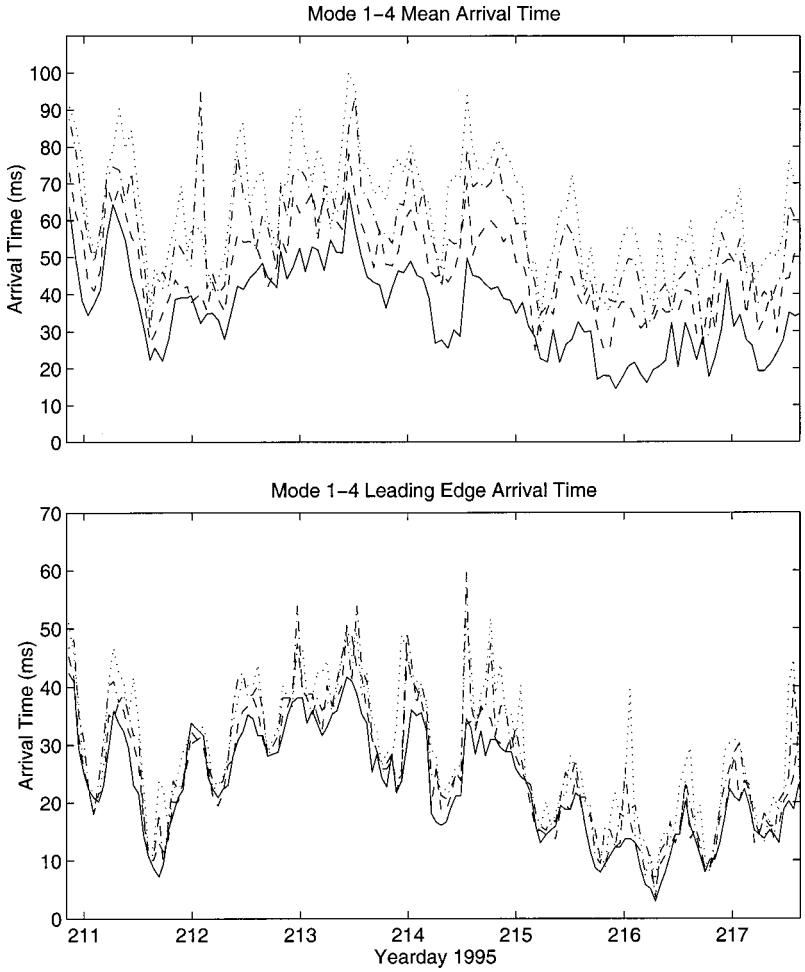


FIG. 12. The lower panel shows plots of the mode one (solid), mode two (dashed), mode three (dot-dashed), and mode four (dotted) peak arrival time distribution leading edges (the plots connect the earliest peak arrivals in 1.1-h bins). The upper frame shows the corresponding 1.4-h bin average mean peak arrival times.

aged mode one spread (IQR) statistics are compared in Fig. 15. Both records exhibit fairly strong M2 tidal modulation of the spread during the first part of the recorded period. The latter portions of both records have more limited tidal signatures, but the modulation that does exist is somewhat similar, and the mean levels of spread exhibited are both about 23 ms above their respective unscattered levels of 7 and 37 ms. (We note that we have included the natural width of the pulse in the spread both in Fig. 15 and our other work, i.e., reported ''total pulse width'' as spread.) The zero-lag cross-correlation between the two entire records is 0.72. The closeness of the spread numbers (23 ms) is easily understood from our receiver dominance argument in the Appendix. The strength of the two-frequency cross-correlation (0.72) needs a more complex picture of the coupled scattering to explain it, and we refer the reader to the papers by Duda and Preisig.[16,24]

### B. Temporal coherence and intensity fluctuations

Given the significant spread observed in the mode-filtered outputs, which implies significant scattering, one would expect to observe fairly short average decorrelation times. To illustrate this, Fig. 16 shows mode 1–4 filtered outputs for five sequences separated by 20 s and five sequences separated by 6 min, over a 30-min period. This figure shows fairly strong correlation between sequences separated by up to 1 min and 22 s; however, the temporal variability over a 6-min period is quite dramatic. The mode pressure amplitude patterns at 6-min lag are basically uncorrelated.

A more quantitative measure of the individual mode temporal coherences can be reached using our data by computing the correlation coefficient between the first sequence (arrival structure) of a transmission and the 20 subsequent sequences in that transmission. Figure 17 displays the results of such computations when averaged over ten transmissions. For the analyzed time period, the average 3-dB down points for the correlation functions fall between 70 and 90 s.

Analysis of this limited number of records tends to confirm suspicions that decorrelation times for the mode arrivals are fairly short, but further analysis shows the decorrelation times themselves to be highly variable. Figure 18 shows the variations of 1.4-h bin averaged 3-dB down decorrelation times for modes 1–4 over a one week period. The broken nature of the data (approximately 2 min of data followed 4 min of silence) is such that quadratic extrapolation is needed to estimate decorrelation times beyond the 107-s point. This extrapolation leads to some large correlation time estimates that are obviously unrealistic; this is an unavoidable error, given our data sampling.

A semidiurnal tidal signature is evident in each of the four plots in Fig. 18. This modulation is a direct consequence of the semidiurnal fluctuations in the distribution of solitons in the waveguide. They cause most of the coupled scattering,

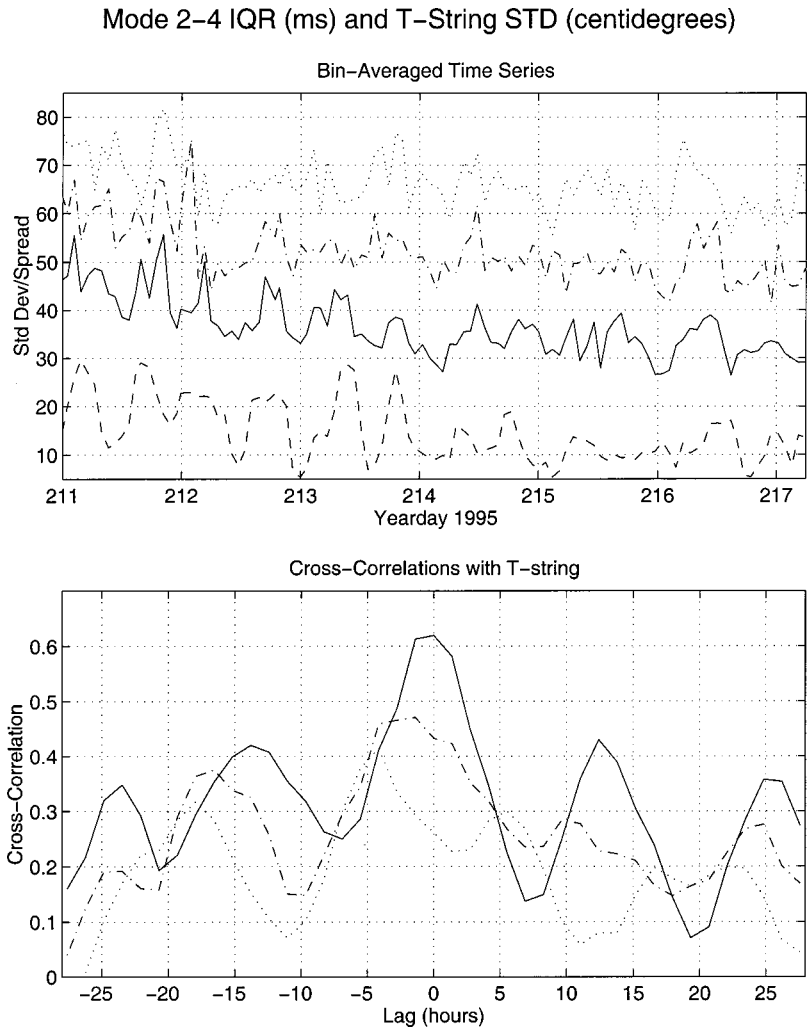


FIG. 13. The upper frame shows a comparison of 1.4-h bin averaged IQR levels for mode two (solid line), mode three (dot-dash line, offset by an additional 10 ms), and mode four (dotted line, offset by an additional 20 ms), and the standard deviation of the temperature at 22.5-m depth over the previous 4.3 h (dashed line). The standard deviation of the temperature is in tenths of a degree C to facilitate comparison with the IQR levels in milliseconds. The lower frame shows the cross-correlation of the temperature statistic with the three bin-averaged spread statistics.

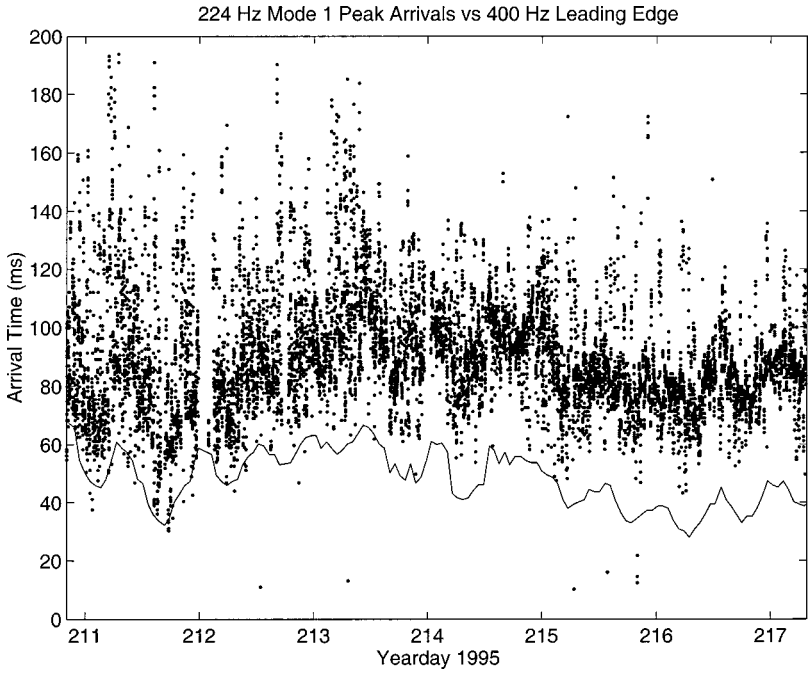


FIG. 14. Distribution of SWARM 224-Hz mode one peak arrival times. The zero reference is at an arrival time of 22.453 s. The plotted transmissions occurred every 5 min. Only 8 sequences (every 4th from 1 to 29) are shown of the 29 available. An upshifted leading edge of the 400-Hz peak arrival distribution is also shown for comparison. The later zero reference time, relative to Fig. 7, stems from the difference in source mooring locations.

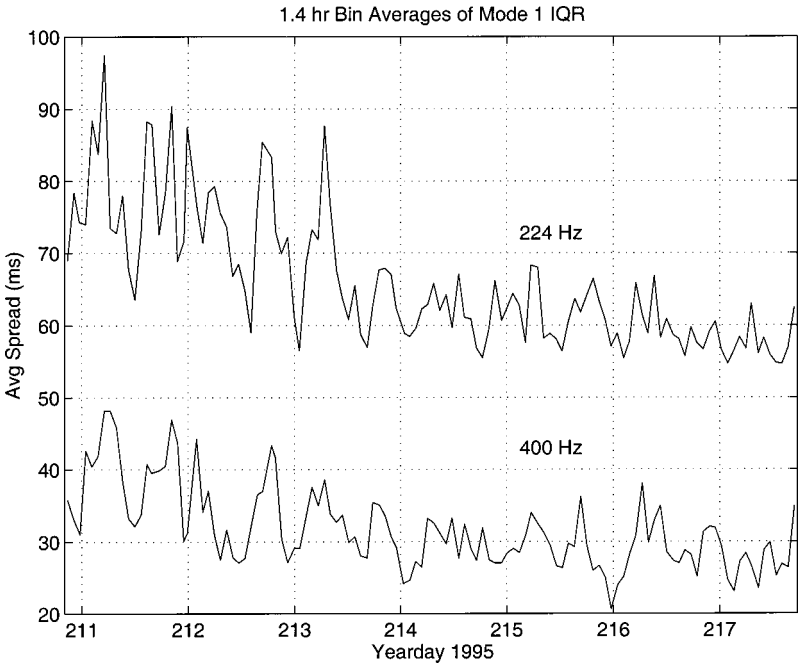


FIG. 15. Comparison of 224-Hz and 400-Hz 1.4-h bin averaged IQR (spread). The IQR pulse width of an unscattered 224-Hz pulse would be about 37 ms (7 ms for a 400-Hz pulse).

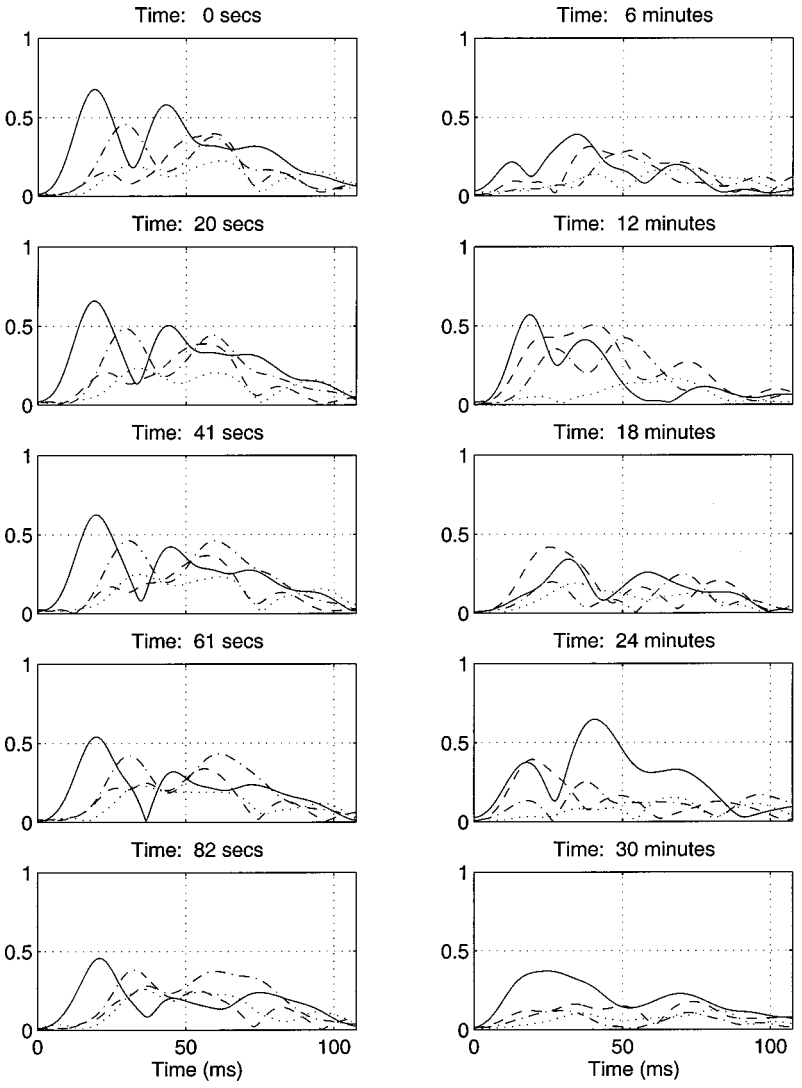


FIG. 16. Mode coefficient outputs, $A_1$ (solid), $A_2$ (dashed), $A_3$ (dot-dash), and $A_4$ (dotted), as a function of time. The five plots in the left column depict the evolution of the mode arrivals over a period of 82 s. The plots in the right hand column depict the evolution of the mode arrivals over a period of 30 min.

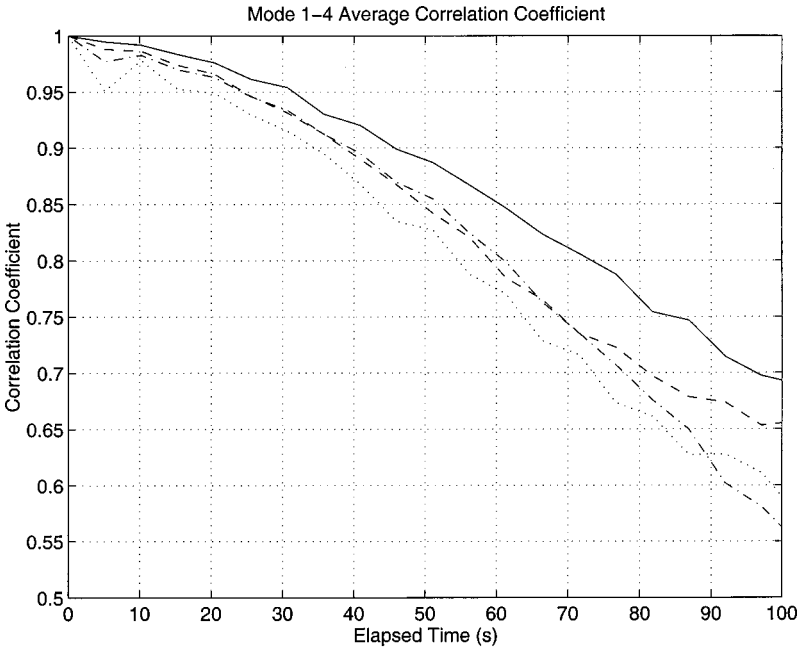


FIG. 17. Average correlation coefficients for outputs, $A_1$ (solid), $A_2$ (dashed), $A_3$ (dot-dash), and $A_4$ (dotted), as a function of elapsed time. The average is taken over the ten transmissions of Fig. 6.

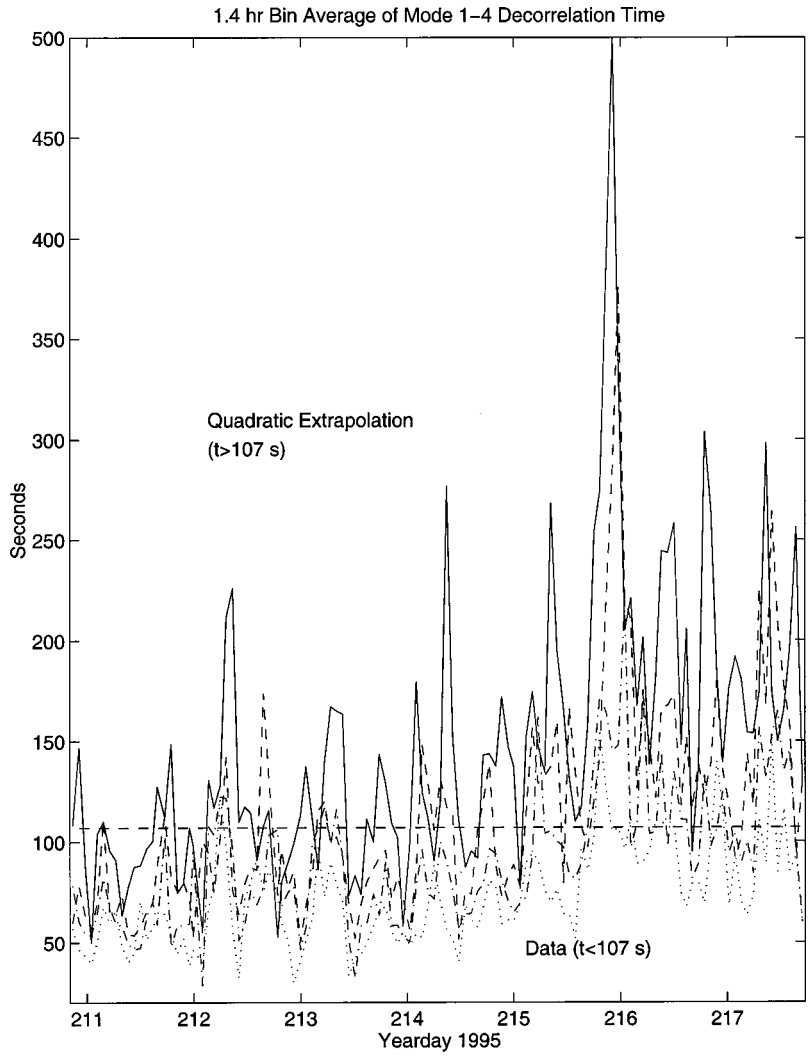


FIG. 18. Decorrelation times for 400-Hz modes 1–4. Mode one is solid, mode two is dashed, mode three is dot-dashed, and mode four is dotted.

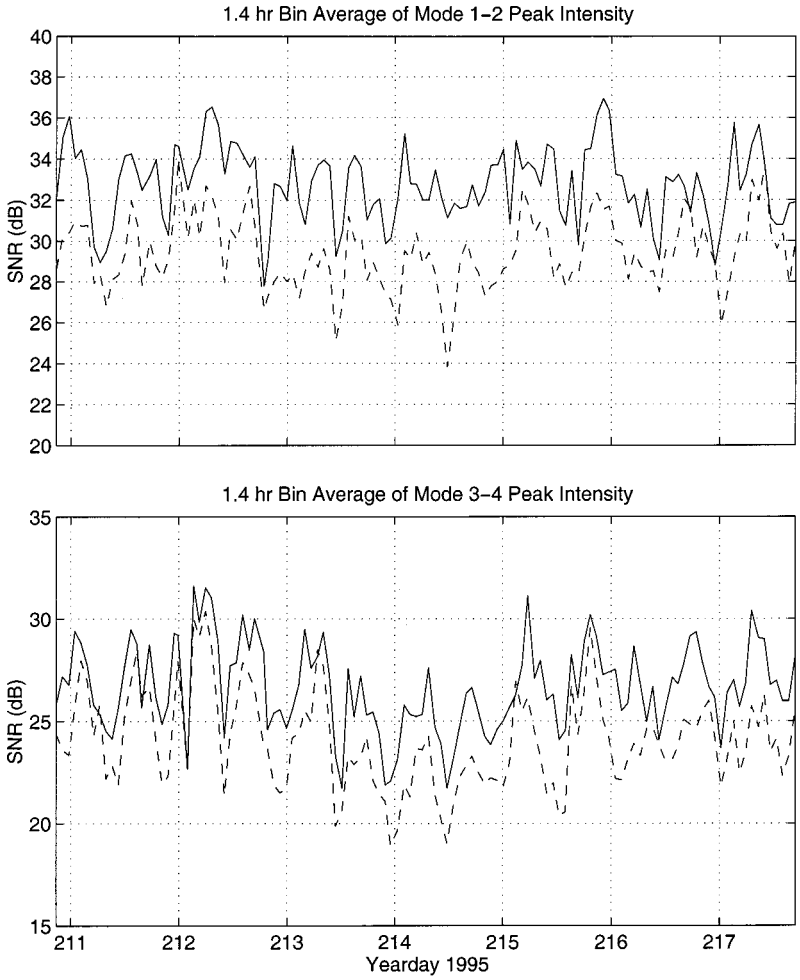


FIG. 19. A comparison of 1.4-h averaged peak-SNR fluctuations for the first four modes of the SWARM data. In the upper frame, mode one is solid and mode two is is dashed. In the lower frame, mode three is solid and mode four is is dashed.

and as the overall amount of mode coupling increases, the level of temporal coherence decreases. The individual mode temporal coherence decrease again correlates well with soliton activity near the receiver.

Increased coupling between modes also affects the peak intensities of the mode arrivals, as evidenced by the strong tidal modulation seen in the Fig. 19 plots of 1.4-h bin averaged peak SNR levels for modes 1–4. Intensities of these lower order modes are reduced as scattering levels increase, so their peak intensity tends to oscillate in phase with temporal coherence and decorrelation time.

The strength of the correlation between the modal intensity and mode decorrelation time appear to increase with mode number, as evidenced by the cross-correlations shown in the upper frame of Fig. 20. The cross-correlation between mode 1–4 peak intensity and our general measure of ''near-receiver'' soliton activity is shown in the middle frame of Fig. 20. Whereas mode one and two *spread* levels were shown to be ''in-phase'' with soliton activity near the receiver (see Figs. 10 and 12), the peak negative correlations with intensity fluctuations occur when the intensities lead (by 2 or 3 h) our soliton activity measurement. One possible explanation for this result is that, given our experimental configuration, solitons from the previous tidal cycle that are near the source are scattering energy from the low modes into the high modes, which are more quickly attenuated. This sensitivity of amplitude effects to soliton activity near the source would also be in agreement with recent numerical studies by Duda and Preisig.[24]

Finally, the plots in the lower frame of Fig. 20 show the cross-correlations between intensity and spread levels for modes 1–4; no phase lags are evident, but only mode one shows a significant negative peak. The mode one result is not too surprising, as its phase lag in the middle panel is only 1.4 h (one unit of resolution).

## IV. SYNOPSIS OF MAIN RESULTS, CONCLUSIONS, AND FUTURE DIRECTIONS

The following conclusions and thoughts on future directions can be drawn from our data analyses.

To begin with, acoustic normal mode arrival time spread and bias, and the modal intensities and decorrelations times measured in the 1995 SWARM experiment show distinct M2 tidal period fluctuations. These are highly correlated to the passage of trains of solitons between the source and receiver. A particular interesting correlation was that of the maximum modal pulse spread with solitons near the acoustic receiver. Although we have not shown it here, there are no other oceanic or bottom acoustic phenomena which can create this same M2 type of signal in our data, so we can reasonably state that these effects *are* due to internal tide solibores. (The interested reader is referred to the thesis by Headrick.[19])

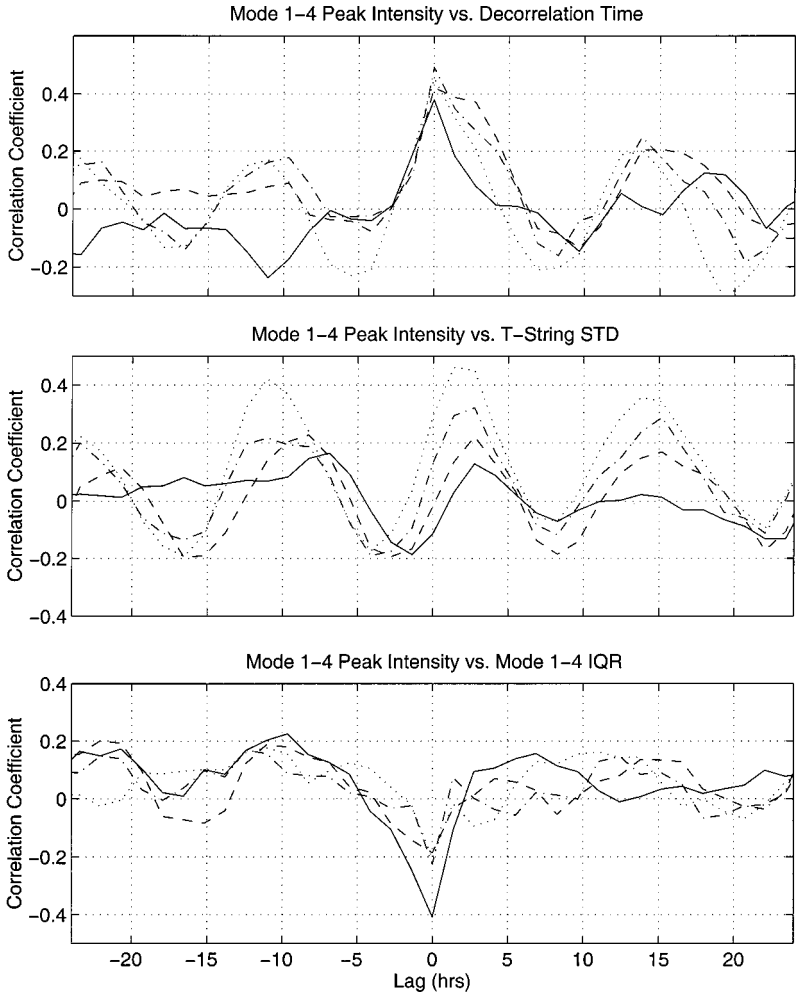


FIG. 20. The upper frame shows cross-correlations between peak intensities and decorrelation times for 400-Hz modes 1–4. The middle frame shows the cross-correlations between mode 1–4 peak intensities and the standard deviation of the temperature at 22.5-m depth over the previous 4.3 h. The lower frame shows the cross-correlations between mode 1–4 peak intensities and the mode 1–4 spread levels (IQR). Mode one is solid, mode two is dashed, mode three is dot-dashed, and mode four is dotted.

Next, under a common shallow water circumstance, i.e., when mode one has the highest group speed, a pseudo-adiabatic mode one (PAM1) arrival time can be estimated from a distribution of peak mode one arrival times by finding the leading edge envelope of the distribution. We saw that mode one had the highest path-averaged group speed for most, if not all, of the duration of the SWARM experiment. This leading edge peak can be very useful for ocean thermometry (or tomography) studies. As an example of this, we observed that large fluctuations in the path-averaged mode one group speed occurred over tidal and subtidal periods during the course of the experiment. A significant percentage of the mode one group speed fluctuations could be attributed to warm water advection in the seaward 5 to 10 km of the SWARM waveguide. This advection, which is probably associated with movement of the foot of the warm, salty shelf-break front, was clearly seen in deep thermistor records near the receiver.

Additionally, although the M2 signal was stressed in this paper, our time series also showed that soliton-filled waveguides produce significant mode arrival structure distortions with fluctuation time scales ranging from minutes to days. We need both better high frequency data and low frequency data to study the 0–10 min and 3 days– 3 months variability signals due to internal waves.

Finally, our data had at least one ''feature'' we wish we could have avoided. The tomography sources and the WVLA receiver were spaced at a distance which corresponds to ~11.2 h for the time of propagation of a soliton train between the two. This is very close to the 12.42-h M2 tidal period at which solitons are generated. Since: (1) the soliton trains have ''time spreads'' of ~3 h to transit a given point, and (2) the times of propagation can also very 10–20 percent due to oceanographic conditions, we often have solitons close to both the source and the WVLA receiver. Thus our data cannot resolve perfectly well whether the acoustic scattering due to solitons was due to solitons near the source or near the receiver. It can, however, distinguish between scattering at the endpoints and scattering in the middle of the path. Working with model predictions has allowed us to resolve this experimental ambiguity to some extent.

As to the future, there are still many gaps that need to be filled in our studies of modal acoustic scattering by soliton-filled ocean waveguides. These include: (1) examining a broader range of acoustic frequencies; (2) obtaining data along a shorter path where the source/receiver scattering ambiguity we encountered does not exist ($R \leqslant 20$ km) (we actually had such a path in our SWARM experiment, but the receiver flooded); (3) examining longer continuous time series of acoustic transmissions (as our 2-min transmissions obviously did not give us quite enough time to fully estimate modal acoustic temporal decorrelation and our one week time series could not see longer term effects such as spring neap cycles); (4) looking at along-shelf propagation paths;

and (5) examining arrivals across a horizontal array. This list is obviously an incomplete one, but represents some of the first order issues the SWARM group sees as important. Our study here also obviously does not encompass full wave acoustic studies, array coherences, or modeling issues—these topics are being pursued, but are beyond the scope of the one pursued in this paper.

## ACKNOWLEDGMENTS

We would first like to heartily acknowledge all of our SWARM collaborators; without their superb efforts, the success of the SWARM experiment would not have been possible. Our principal Office of Naval Research sponsor, Dr. Jeff Simmen, is also warmly acknowledged for his strong support of the project. The support of Dr. Lou Goodman of ONR for some of the oceanographic analyses is gratefully acknowledged as well. The funds for the data analyses by R. Headrick were provided by the Office of Naval Research through an ONR Fellowship (Massachusetts Institute of Technology award 002734-001); the general funds for SWARM were provided by the Office of Naval Research through ONR Grant No. N00014-95-0051. This is Woods Hole Oceanographic Institution contribution number 10076.

## APPENDIX: A SIMPLE MODEL OF PULSE BROADENING DUE TO NEAR RECEIVER MODE COUPLING

One of the major results that our SWARM experimental work indicates is ''near-receiver dominance'' of the time spreading of acoustic pulses by soliton scattering. This sensitivity of the time spreading to near-receiver mode coupling is also seen clearly in the rather elaborate numerical modeling efforts by Headrick *et al.*[19,22] However, there is an even simpler way to see how this effects works physically in the context of an simple, two-coupled-mode ''toy'' model. Such a model allows one to show *analytical* forms for the modal time spreading versus the distance along the acoustic path of the acoustic mode coupler (in this case a train of solitons).

To begin with, let us consider a two mode system, with trapped modes one and two present only. Mode one is the faster mode, with group speed $v_1^G > v_2^G$. Also, let us assume that mode one has a very small modal attenuation coefficient, $\beta_1 \simeq 0$, whereas $\beta_2$ is somewhat larger ($\beta_2 \neq 0$). For the coupling matrix, no assumption is really necessary, as it is an amplitude effect. One can assume equal coupling into and out of the two modes for simplicity, if desired.

We now look at the propagation from the source at $x=0$ to the receiver at $x=L$. For mode one, the time of flight is $L/v_1^G = t_1$; for mode two we get $L/v_2^G = t_2$. Now let's consider looking at time spread arrivals in mode one where we can have both an unscattered arrival (travel is purely in mode one) and a single scattered arrival (one coupling by the soliton from mode two to mode one occurs at some distance $x$ along the path from source-to-receiver) comprising the spread arrival. The time spread between the initial mode one arrival at $t_1 = L/v_1^G$ and the later scattered arrival is

$$\Delta t_1 = |L/v_1^G - (x/v_2^G + (L-x)/v_1^G)|. \tag{A1}$$

The amplitude (ignoring the coupling strength and spreading, and just including modal attenuation for simplicity) of the single coupled mode arrival is

$$A_1 = A_1^0 e^{-\beta_2 x}. \tag{A2}$$

Clearly Eq. (A1) gives the greatest time spread of the pulse when $x=L$, i.e., when the scattering is near the receiver. However, there is a decrease in amplitude of the single scattered arrival, which produces a *minimum* amplitude when $x=L$ in this case. Thus there is some trade-off between time spread maximization (best at $x=L$) and scattered arrival amplitude maximization (best at $x=0$). In the case of the mode two arrivals, things are in fact a bit more favorable to ''near-receiver dominance.'' The time spread between the unscattered mode two arrival and the (faster) coupled mode arrival is simply expressed as

$$\Delta t_2 = |L/v_2^G - (x/v_1^G + (L-x)/v_2^G)|, \tag{A3}$$

which again is a maximum when $x=L$. The amplitude of the single scattered coupled mode arrival is

$$A_2 = A_2^0 e^{-\beta_2 (L-x)}. \tag{A4}$$

The amplitude in Eq. (A4) is clearly a *maximum* when $x=L$, thus giving the maximum amplitude for the scattered arrival when the scatterer is near the receiver.

The above argument gives the simple physical rationale for why near-receiver scattering produces the most time spread, but does not pretend to handle the details of the scattering, propagation, or coupling in any exact sense. For these details, we refer the reader to the thesis and modeling paper by Headrick *et al.*[19,22]

[1] J. X. Zhou, X. Z. Zhang, and P. H. Rogers, ''Resonant interaction of sound wave with internal solitons in the coastal ocean,'' J. Acoust. Soc. Am. **90**, 2042–2054 (1991).
[2] J. X. Zhou, X. Z. Zhang, P. H. Rogers, D. Wang, and E. Luo, ''Anomalous sound propagation in shallow water due to internal wave solitons,'' Proc. IEEE Oceans '93 **1**, 87–92 (1993).
[3] D. B. King, S. A. Chin-bing, and R. W. McGirr, ''Ocean variability and acoustic propagation,'' in *Theoretical and Computational Ocean Acoustics*, Vol. 2, edited by D. Lee and M. Schultz (World Scientific, Singapore, 1994), pp. 793–807.
[4] M. K. Broadhead and H. B. Ali, ''Dissipative shallow water internal waves and their acoustical properties,'' Proc. MTS/IEEE Oceans '95 (IEEE, 1995).
[5] The SWARM Group (J. R. Apel *et al.*), ''An overview of the 1995 SWARM shallow water internal wave acoustic scattering experiment,'' IEEE J. Ocean Eng. **22**, 465–500 (1997).
[6] D. Rubenstein, ''Observations of cnoidal internal waves and their effect on acoustic propagation in shallow water,'' J. Acoust. Soc. Am. **101**, 3016 (1997).
[7] X. Demoulin, Y. Stephan, E. Coelho, S. Jesus, and M. B. Porter, ''Intimate96: A shallow water tomography experiment devoted to the study of internal tides,'' in *Shallow-Water Acoustics*, edited by R. Zhang and J. Zhou (China Ocean Press, Beijing, April 21–25, 1997), pp. 485–490.
[8] G. G. Gawarkiewicz, R. Pickart, J. F. Lynch, C. S. Chiu, K. B. Smith, and J. H. Miller, ''The shelfbreak front PRIMER experiment,'' J. Acoust. Soc. Am. **101**, 3016 (1997).
[9] J. F. Lynch, G. G. Gawarkiewicz, C. S. Chiu, R. Pickart, J. H. Miller, K. B. Smith, A. Robinson, K. Brink, R. Beardsley, B. Sperry, and G. Potty, ''Shelfbreak PRIMER—An integrated acoustic and oceanographic field study in the Mid-Atlantic Bight,'' in *Shallow-Water Acoustics*, edited by R. Zhang and J. Zhou (China Ocean Press, Beijing, April 21–25, 1997), pp. 205–212.
[10] R. L. Field, C. Mire, Z. Hallock, J. George, and M. Broadhead, ''The SESAME experiments—the effects of internal solitons on acoustic propa-

gation at the Malin Shelf,'' in *Shallow-Water Acoustics*, edited by R. Zhang and J. Zhou (China Ocean Press, Beijing, April 21–25, 1997), pp. 227–232.
[11] P. F. Worcester, U. Send, B. D. Cornuelle, and C. Tiemann, ''Acoustic monitoring of flow through the Strait of Gibraltar,'' in *Shallow-Water Acoustics*, edited by R. Zhang and J. Zhou (China Ocean Press, Beijing, April 21–25, 1997), pp. 471–478.
[12] J. X. Zhou, P. H. Rogers, G. W. Caille, R. Zhang, G. Jin, L. Lei, P. H. Dahl, R. C. Spindel, and Z. Gan, ''Overview of the joint China-U.S. ''Yellow Sea '96'' experiment,'' in *Shallow-Water Acoustics*, edited by R. Zhang and J. Zhou (China Ocean Press, Beijing, April 21–25, 1997), pp. 17–22.
[13] D. B. Creamer, ''Scintillating shallow water waveguides,'' J. Acoust. Soc. Am. **99**, 2825–2838 (1996).
[14] D. Tielbuerger, S. Finette, and S. Wolf, ''Acoustic propagation through an internal wave field in a shallow water waveguide,'' J. Acoust. Soc. Am. **101**, 789–808 (1997).
[15] X. Tang and F. D. Tappert, ''Effects of internal waves on sound pulse propagation in the Straits of Florida,'' IEEE J. Ocean Eng. **22**, 245–255 (1997).
[16] J. Preisig and T. F. Duda, ''Coupled acoustic mode propagation through continental shelf internal solitary waves,'' IEEE J. Ocean Eng. **22**, 256–269 (1997).
[17] M. B. Porter, ''The KRAKEN normal mode program,'' Technical report, SACLANT Undersea Research Center, November 1992.
[18] F. B. Jensen, W. A. Kuperman, M. B. Porter, and H. Schmidt, *Computational Ocean Acoustics* (American Institute of Physics, New York, 1994).
[19] R. H. Headrick, ''Analysis of internal wave induced mode coupling effects on the 1995 SWARM acoustic transmissions,'' Ph.D. thesis, MIT/WHOI Joint Program in Oceanography and Oceanographic Engineering, June 1997.
[20] D. Rubenstein and M. H. Brill, ''Acoustic variability due to internal waves and surface waves in shallow water,'' in *Ocean Variability and Acoustic Propagation*, edited by J. Potter and V. Warn-Varnas (Kluwer Academic, Boston, 1991), pp. 215–228.
[21] F. S. Henyey and A. Hoering, ''Energetics of borelike internal waves,'' J. Geophys. Res. **102**, 3323–3330 (1997).
[22] R. H. Headrick, J. F. Lynch, and the SWARM group, ''Modeling mode arrivals in the 1995 SWARM experiment acoustic transmissions,'' J. Acoust. Soc. Am. (submitted).
[23] J. R. Apel, S. I. Finette, M. H. Orr, and J. F. Lynch, ''The ''dnoidal'' model for internal solitons and tides on the continental shelf,'' J. Geophys. Res. (submitted).
[24] T. F. Duda and J. Preisig, ''Acoustic effects of moving coastal solitary wave packets,'' IEEE J. Ocean Eng. **24**, 16–32 (1999).